

Extracting Separation Surfaces of Path Line Oriented Topology in Periodic 2D Time-Dependent Vector Fields

Kuangyu Shi
MPI Informatik
66123 Saarbrücken, Germany
skyshi@mpi-inf.mpg.de

Helwig Hauser
VRVis Research Center
1220 Vienna, Austria
hauser@vrvis.at

Holger Theisel
Bielefeld University
33501 Bielefeld, Germany
theisel@techfak.uni-bielefeld.de

Hans-Christian Hege
Zuse Institute Berlin
14159 Berlin, Germany
hege@zib.de

Tino Weinkauff
Zuse Institute Berlin
14159 Berlin, Germany
weinkauff@zib.de

Hans-Peter Seidel
MPI Informatik
66123 Saarbrücken, Germany
hpseidel@mpi-inf.mpg.de

ABSTRACT

This paper presents an approach to extracting the separation surfaces from periodic 2D time-dependent vector fields based on a recently introduced path line oriented topology. This topology is based on critical path lines which repeat the same spatial cycle per time period. Around those path lines there are areas of similar asymptotic flow behavior (*basins*) which are captured by a 2D Poincaré map as a discrete dynamical system. Due to pseudo discontinuities in this map and the discrete integration scheme, separatrices between the basins can't be obtained as integral curves. Instead we choose a point-wise approach to segment the Poincaré map and apply image analysis algorithms to extract the 2D separation curves. Starting from those curves we integrate separation surfaces which partition the periodic 2D time-dependent vector field into areas of similar path line behavior. We apply our approach to a number of data sets to demonstrate its utility.

Keywords: Flow Visualization, Time-dependent vector fields, Topological methods.

1 INTRODUCTION

Over the last decade, topological methods have become standard in vector field visualization. Initially introduced as a visualization tool in [6], topological methods have been extended to higher order critical points [12], boundary switch points [1], and closed trajectories [30]. In addition, methods have been proposed to simplify flow topology [1, 2, 21, 22, 28]. Also topological methods have been presented to smooth [29], compress [8, 17] and construct [16, 26] vector fields. The topology of 3D vector fields has also been used for visualization [4, 9, 11, 19, 25].

The main idea behind topological methods is to segment a vector field into areas of similar asymptotic behavior. This means classifying each point \mathbf{x} in the domain with respect to the asymptotic behavior of the flow trajectory through it, i.e., a forward and backward integration starting from \mathbf{x} with an integration time converging to infinity is considered. Usually, this integration does not have to be carried out for every point but only for a certain number of starting points of separatrices.

Permission to make digital or hard copies of all or part of this work for personal or classroom use is granted without fee provided that copies are not made or distributed for profit or commercial advantage and that copies bear this notice and the full citation on the first page. To copy otherwise, or republish, to post on servers or to redistribute to lists, requires prior specific permission and/or a fee.
Copyright UNION Agency – Science Press, Plzen, Czech Republic.

For time-dependent vector fields there exists a number of relevant integration curves, such as stream lines, path lines, streak lines and time lines. Among them, stream lines, and path lines have the uniqueness property: through each point in the space-time domain there is exactly one stream line and exactly one path line. This means that two different kinds of topologies can be considered: a stream line oriented topology segmenting areas of similar stream line behavior, and a path line oriented topology which does so for path lines. Extracting a stream line oriented topology ends up in tracking critical points and considering certain bifurcations [23, 31, 18, 3, 20].

Path lines are important structures in time-dependent vector fields because they describe the paths of massless particles in the flow. Hence, a path line oriented segmentation gives a different kind of insight into the vector field data than the stream lines oriented variants. One can even argue that a path line oriented flow topology is more truthful to intrinsic characteristics of the flow. Theisel et al. consider the *local* topological behavior by segmenting the domain into regions of locally attracting, repelling, or saddle-like path lines [20]. As the practical experience, many real or simulated time-dependent vector fields are periodic or quasi periodic. Shi et al. present a point based approach to extract the *asymptotic* path line behavior of periodic 2D time-dependent vector fields [13]. This approach uses a Poincaré map as a discrete dynamical system to detect critical path lines as well as basins from which path lines converge to the critical cycles. However, within

this approach basins can only be computed for a given time slice. A segmentation of the whole 3D space-time domain is missing. This is due to the fact that separatrices between the basins can not be obtained as integral curves, because of the discrete integration scheme and certain pseudo discontinuities in the Poincaré map.

This paper extends this work [13] by presenting an approach to extract the separatrices of the Poincaré map using algorithms from the field of image analysis. Once those 2D separation curves are extracted, the segmentation of the whole 3D space-time domain can be obtained by a stream surface integration starting at the separatrices of the Poincaré map.

The rest of the paper is organized as follows: Section 2 recalls the concepts of path line oriented topology for periodic time-dependent vector fields. Section 3 analyzes the difficulties in calculating the separation surfaces using classical topological methods. Section 4 describes how to extract the separation curves of the Poincaré map for a given time step and presents a stream surface integration algorithm with error correction to obtain the separation surfaces for the whole 3D space-time domain. Section 5 outlines our algorithm for extracting the topological skeleton. Section 6 shows a number of applications of our approach, while conclusions are drawn in section 7.

2 PATH LINE ORIENTED TOPOLOGY FOR PERIODIC VECTOR FIELD

Given a 2D time-dependent vector field $\mathbf{v}(\mathbf{x}, t)$ in the space-time domain $D \times [t_{min}, t_{max}]$ with $D = [x_{min}, x_{max}] \times [y_{min}, y_{max}]$, then \mathbf{x} describes a point in the spatial domain and t is the respective temporal component.

A path line oriented topological segmentation of \mathbf{v} can't be made by applying conventional topological methods of 3D vector fields because an integration of a path line until infinity is impossible due to the finite temporal domain. This restriction is no longer valid when considering periodic vector fields. And periodic or quasi periodic vector fields is one of the main categories of time-dependent vector fields in scientific visualization. So it is reasonable to focus our consideration on periodic time-dependent vector fields.

Assume that \mathbf{v} describes one period, with $\mathbf{v}(\mathbf{x}, t_{min}) = \mathbf{v}(\mathbf{x}, t_{max})$. Then it is sufficient to consider this period which can be repeated as often as necessary. We can assume \mathbf{v} to be defined in the whole domain $D \times \mathbb{R}$ by setting

$$\mathbf{v}(\mathbf{x}, t) = \mathbf{v}(\mathbf{x}, t + k \Delta t),$$

where $\Delta t = (t_{max} - t_{min})$ and k is an integer chosen such that $t_{min} \leq t + k \Delta t < t_{max}$.

In order to integrate a path line in the periodic field \mathbf{v} , two equivalent strategies can be applied:

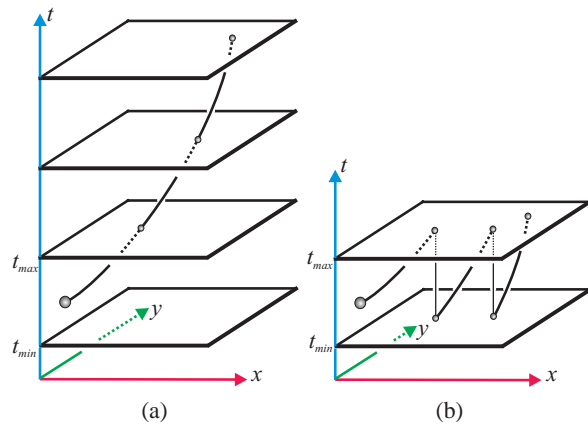


Figure 1: Two equivalent approaches of a stream line integration in a periodic field \mathbf{v} : (a) In the unbounded time-domain; (b) Periodically continued in the time-domain $[t_{min}, t_{max}]$.

- The integration is done over the unbounded time-domain as illustrated in figure 1a.
- If the integration approaches a point (\mathbf{x}, t_{max}) , it is mapped to (\mathbf{x}, t_{min}) . From there, the integration is continued until t_{max} is reached again. Figure 1b illustrates this.

Instead of integrating path lines directly, the point based approach of topological path line segmentation [13] constructs two 2D Poincaré maps to analyze the asymptotic behavior of those path lines starting at certain times.

2.1 2D Poincaré maps

Picking a certain reference time τ with $t_{min} \leq \tau < t_{max}$, two 2D maps $\mathbf{m}_\tau(\mathbf{x})$ and $\bar{\mathbf{m}}_\tau(\mathbf{x})$ are constructed for the segmentation of the asymptotic behavior of all path lines starting at the time τ . For $\mathbf{m}_\tau(\mathbf{x})$, a forward integration of \mathbf{v} from (\mathbf{x}, τ) is carried out until one of the following cases occurs:

1. The integration reaches the time level $\tau + \Delta t$, i.e. it comes to a certain point $(\mathbf{x}_f, \tau + \Delta t)$. Then $\mathbf{m}_\tau(\mathbf{x})$ is set to \mathbf{x}_f .
2. The integration leaves D before reaching the level $\tau + \Delta t$. In this case $\mathbf{m}_\tau(\mathbf{x})$ is marked as undefined.

In a similar way, $\bar{\mathbf{m}}_\tau(\mathbf{x})$ is defined by starting a backward integration of \mathbf{v} from (\mathbf{x}, τ) until the time level $\tau - \Delta t$ is reached at a point $(\mathbf{x}_b, \tau - \Delta t)$, or until the integration leaves D . Figure 2a illustrates the definitions of $\mathbf{m}_\tau(\mathbf{x})$ and $\bar{\mathbf{m}}_\tau(\mathbf{x})$.

Instead of the definition of the maps $\mathbf{m}_\tau(\mathbf{x})$ and $\bar{\mathbf{m}}_\tau(\mathbf{x})$ as described above, a vector-oriented, relative description of the map can also be used:

$$\begin{aligned} \mathbf{q}_\tau(\mathbf{x}) &= \mathbf{m}_\tau(\mathbf{x}) - \mathbf{x} \\ \bar{\mathbf{q}}_\tau(\mathbf{x}) &= \bar{\mathbf{m}}_\tau(\mathbf{x}) - \mathbf{x} \end{aligned} \quad (1)$$

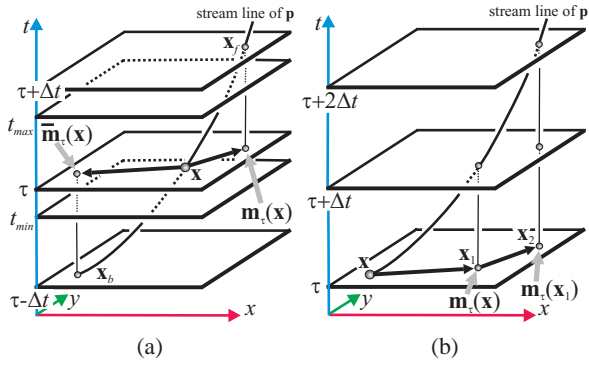


Figure 2: (a) The definition of $\mathbf{m}_\tau(\mathbf{x})$ and $\bar{\mathbf{m}}_\tau(\mathbf{x})$; (b) A continuous forward integration of \mathbf{v} corresponds to a discrete integration of $\mathbf{m}_\tau(\mathbf{x})$.

$\mathbf{m}_\tau(\mathbf{x})$ and $\mathbf{q}_\tau(\mathbf{x})$ and all of the related considerations in the remainder of this paper can be easily transformed into each other.

The maps \mathbf{m}_τ and $\bar{\mathbf{m}}_\tau$ can be interpreted as 2D Poincaré maps [10]. In order to analyze the asymptotic behavior of a path line starting from (\mathbf{x}, τ) in forward direction, we do not have to integrate \mathbf{v} any more but can restrict ourselves to a sequence of maps of $\mathbf{m}_\tau(\mathbf{x})$:

$$\begin{aligned} \mathbf{x}_0 &= \mathbf{x} \\ \mathbf{x}_{i+1} &= \mathbf{m}_\tau(\mathbf{x}_i) \end{aligned} \quad (2)$$

and considering the asymptotic behavior for $i \rightarrow \infty$. Figure 2b illustrates this relation. A similar statement holds for the backward integration of \mathbf{v} and a sequence of maps of $\bar{\mathbf{m}}_\tau$.

2.2 Point based topological segmentation of 2D Poincaré map

The segmentation of areas of similar path line behavior corresponds to the topological segmentation of the 2D Poincaré maps \mathbf{m}_τ and $\bar{\mathbf{m}}_\tau$, respectively. Critical path lines in \mathbf{v} correspond to fixed points in \mathbf{m}_τ and $\bar{\mathbf{m}}_\tau$. They may act as sources, sinks, or saddle path lines building α - and ω -basins in D .

The point-wise approach is applied as follows: for every point \mathbf{x} in D , an integration of \mathbf{m}_τ is carried out using (2) until one of the following conditions is fulfilled:

- \mathbf{x}_i comes close to a fixed point of \mathbf{m}_τ ,
- \mathbf{x}_i leaves the domain D ,
- i exceeds a certain maximal threshold.

In the first case, \mathbf{x} is assumed to be part of the basin of the fixed point. This means that the path line starting at (\mathbf{x}, τ) converges to a critical path line under forward integration. In the second case, the path line is known to leave the domain under forward integration. In the last case, \mathbf{x} is marked as unknown. A similar procedure is applied for the segmentation of backward Poincaré map $\bar{\mathbf{m}}_\tau$.

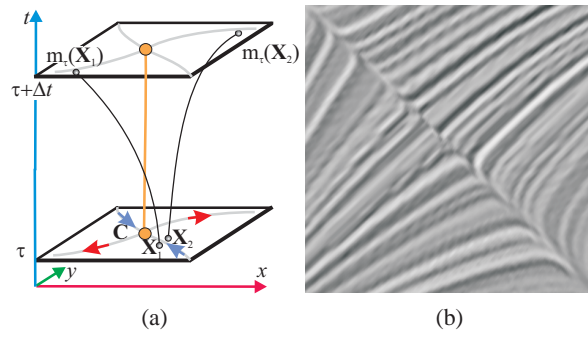


Figure 3: Pseudo discontinuities in \mathbf{m}_τ : (a) If \mathbf{x}_1 and \mathbf{x}_2 are close but at different sides of a separatrix of $\mathbf{v}(\mathbf{x}) = \mathbf{v}(\mathbf{x}, t)$, \mathbf{m}_τ has too large changes that it is impossible for discrete numerical method to deal with it though it is still continuous; (b) The pseudo discontinuity in corresponding Poincaré map.

3 DIFFICULTIES WITH SEPARATION SURFACE EXTRACTION

In the point based approach [13], the topological segmentation of path lines starting at a certain time is successfully computed. However, this is still not the classical topological structure of the whole data set. The computation for every considered time is time consuming, so the separation surfaces are needed to present the general path line oriented topological structure.

However it is difficult to generate the separation surfaces. The discrete integration and the pseudo discontinuity of a Poincaré map are two key problems for classical topological method when extracting separation surfaces.

3.1 Discrete dynamic systems

Both Poincaré maps \mathbf{m}_τ and $\bar{\mathbf{m}}_\tau$ can be considered as discrete invertible dynamical systems. As shown in equation (2), the integration of Poincaré maps is equivalent to a numerical Euler integration of \mathbf{q}_τ with step size 1: $\mathbf{x}_{i+1} = \mathbf{x}_i + 1 \mathbf{q}_\tau(\mathbf{x}_i)$.

For discrete dynamical systems, classical topological vector field approaches fail to give the correct segmentation because they reflect continuous dynamical systems. For continuous dynamical systems, the different basins are separated by stream lines starting from saddle points. However, such a stream line integration does not exist for the discrete systems \mathbf{m}_τ and $\bar{\mathbf{m}}_\tau$.

Note that the topology of discrete dynamical systems can get a lot more complicated, even for lower dimensions, when compared to the continuous case.

3.2 Pseudo discontinuity

Although \mathbf{v} is continuous, both \mathbf{m}_τ and $\bar{\mathbf{m}}_\tau$ may have pseudo discontinuities, which means that \mathbf{m}_τ and $\bar{\mathbf{m}}_\tau$ are still continuous mathematically, but they may have areas with tremendous large gradient, which appear as discontinuities for discrete treatment. To see this point,

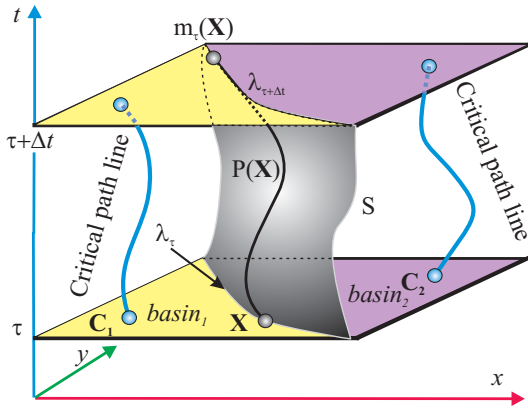


Figure 4: The relation between the basin edges and the separation surfaces for asymptotical path line behavior.

we consider the example of a steady 2D vector field $\mathbf{v}(\mathbf{x}) = \mathbf{v}(\mathbf{x}, t)$ which can also be considered as a periodic time-dependent vector field. Setting a certain time Δt as period, $\mathbf{m}_\tau(\mathbf{x})$ is obtained by a stream line integration of \mathbf{v} at \mathbf{x} over a time Δt . If \mathbf{v} consists of saddles, its separatrices may induce tremendous changes in \mathbf{m}_τ so that it appears as discontinuities for normal discrete numerical programs. Figure 3 illustrates this.

4 TOPOLOGICAL SEPARATION SURFACE EXTRACTION

If we integrate the edges of the segmentation basins obtained from point based method (section 2.2) either in forward or backward directions, we could get the separation surfaces for the asymptotic behavior of corresponding path lines.

For a given periodic 2D time-dependent vector field \mathbf{v} , suppose we have extracted the separation surface S and at time τ , we have obtained the basin segmentation using point based method. λ_τ is the intersection curve of S and plane $t = \tau$. It is obvious that λ_τ exactly coincides with the edges of the segmentation basins in τ and λ_τ exactly coincides with $\lambda_{\tau+\Delta t}$. For any point \mathbf{x} in λ_τ , if we integrate a path line $\mathbf{P}(\mathbf{x})$, we can conclude that $\mathbf{P}(\mathbf{x})$ coincides in S within the domain and $\mathbf{m}_\tau(\mathbf{x})$ coincides $\lambda_{\tau+\Delta t}$ after a period at time $\tau + \Delta t$ if $\mathbf{m}_\tau(\mathbf{x})$ does not leave the domain. Thus, the integration surface of λ_τ coincides with S . Otherwise, $\mathbf{m}_\tau(\mathbf{x})$ would end up either in $basin_1$ or $basin_2$, then \mathbf{x} must also be classified either $basin_1$ or $basin_2$ since it asymptotically converges to critical path lines either in $basin_1$ or $basin_2$, which results in a contradiction. Note that $\mathbf{m}_\tau(\mathbf{x})$ does not necessary equal \mathbf{x} , though it must falls in λ_τ . Figure 4 illustrates this relation.

Here the problem of extraction of separation surface turns to the detection of basin edges as seeding curves and the integration of these seeding curves to surfaces.

-1	0	1
-2	0	2
-1	0	1

G_x

1	2	1
0	0	0
-1	-2	-1

G_y

Figure 5: Sobel Operator.

4.1 Seeding curve detection

We apply an image analysis approach to detect the basin edges.

The basin edges are step discontinuities where the image intensity abruptly changes from one value to another. Many algorithms have been developed to detect such edges [5, 7]. Wallisch applied an extended marching cube approach to extracting the basin boundaries of 3D dynamical systems [24]. Since we aim at a special problem, we apply one simple algorithm here.

Suppose the basin image is $f(x, y)$ in domain $D = [x_{min}, x_{max}] \times [y_{min}, y_{max}]$, where $f(x, y)$ is the id values for different basins. The gradient at location (x, y) is defined as follows:

$$\nabla f = \begin{pmatrix} G_x \\ G_y \end{pmatrix} = \begin{pmatrix} \frac{\partial f}{\partial x} \\ \frac{\partial f}{\partial y} \end{pmatrix} \quad (3)$$

the magnitude of the gradient vector is denoted $g(x, y)$ where

$$g(x, y) = |\nabla f| = \sqrt{G_x^2 + G_y^2} \quad (4)$$

Let $\alpha(x, y)$ represent the direction angle of the gradient vector with respect to the x -axis.

$$\alpha(x, y) = \arctan\left(\frac{G_y}{G_x}\right) \quad (5)$$

The direction of an edge at (x, y) is perpendicular to the direction of the gradient vector.

Here, for the discrete case, we use Sobel operator to calculate the gradient vector as shown in figure 5 [5].

We analyze the characteristics of pixels in a small neighborhood (say, 3×3 or 5×5) about every point (x, y) in the basin image. Thus an edge pixel with coordinates (x_0, y_0) in the predefined neighborhood of (x, y) is similar in magnitude to the pixel at (x, y) if

$$|g(x, y) - g(x_0, y_0)| \leq E \quad (6)$$

where E is a nonnegative threshold. Similarly (x_0, y_0) has similar direction as (x, y) if

$$|\alpha(x, y) - \alpha(x_0, y_0)| \leq A \quad (7)$$

where A is a nonnegative threshold.

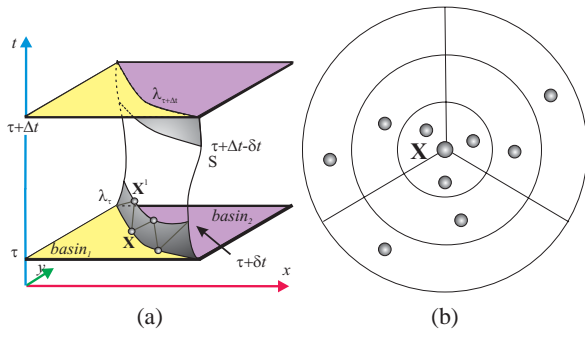


Figure 6: (a) The integration of seeding curves with super sampling in both forward and backward direction until they meet each other; (b) The polar stratified super sampling: $n \times n$ subdivide the circular neighborhood in both radius and angle direction, for each subdivided grid, randomly select a point as sample point.

A point in the predefined neighborhood of (x, y) is linked to the pixel at (x, y) if both magnitude and direction similarity criteria are satisfied. This process is repeated at every location in the basin image and finally we obtain the edges of the basins.

4.2 Step advancing integration with super sampling adjustment

With the detected seeding curve, the classical stream surface integration method is applied to generate the separation surface. However the pseudo discontinuity (section 3.2) makes the integration quite unstable: a small error in the seeding curve may cause large error in the integration.

Here we apply step advancing integration in both forward and backward direction until they meet each other. In each integration step we use super sampling to adjust the result position. Figure 6 illustrates this. We divide period Δt into small steps δt , and integrate the surface step by step. For a seeding point \mathbf{x} in the seeding curve λ , we consider a small circular neighborhood around it and use polar stratified sampling (as shown in Figure 6b) to select the sample points, we integrate all these sample points for δt , and compare the end positions of them to collect the adjusted sampling result \mathbf{x}^1 . Two strategies can be used to collect the adjusted result: (1) closest point to the neighbor adjusted result; (2) the average of sample end points in the most frequent area. In practice we haven't found significant differences between these two sample collection strategies. With the adjusted sampling result, we can integrate step by step further until the final surface is obtained.

5 THE ALGORITHM

In this section we formulate our algorithm to extract the path line oriented topological segmentation surface of a periodic 2D vector field $\mathbf{v}(\mathbf{x}, t)$:

1. Pick a time τ with $t_{min} \leq \tau < t_{max}$ for which we compute the topological segmentation.
2. Compute the Poincaré maps \mathbf{m}_τ and $\bar{\mathbf{m}}_\tau$, or equivalently, the vector fields \mathbf{q}_τ and $\bar{\mathbf{q}}_\tau$ [13].
3. Extract the fix points of \mathbf{m}_τ and $\bar{\mathbf{m}}_\tau$ and classify them [13].
4. Generate the topological segmentation at time τ in both forward and backward direction using point based method [13].
5. Extract the edges of both the forward and backward segmentation basins as seeding curves.
6. Integrate the forward seeding curves in both forward and backward direction until the separation surfaces of forward asymptotic path line behavior for a whole period is obtained.
7. Similar to 6 for separation surfaces of backward asymptotic path line behavior.

Note that the extracted edges may have small jags, before integrating the separation surfaces, we must smooth them. Here we apply the Gaussian filter to smooth the edges.

6 APPLICATIONS

In this section we apply our technique to a number of test data sets.

Figure 7 and figure 9a-c illustrate our technique at a random vector field. We use random fields as a proof-of-concept because they contain a maximal amount of topological information. The vector field is piecewise trilinear over a $7 \times 7 \times 7$ grid where the time i -th and the $(6-i)$ th time slices coincide for $i = 0, \dots, 2$. Figure 9a shows the visualization of \mathbf{v} using LIC planes at three different time slices as well as a number of illuminated stream lines. Figure 7a-7b show the 2D vector fields \mathbf{q}_τ and $\bar{\mathbf{q}}_\tau$ which correspond to the Poincaré maps \mathbf{m}_τ and $\bar{\mathbf{m}}_\tau$ for $\tau = t_{min}$. The LIC images reveal the pseudo discontinuities in the Poincaré maps. However, the LIC images also present information about the stream lines of \mathbf{q}_τ and $\bar{\mathbf{q}}_\tau$. Since only a discrete integration is carried out, stream lines of \mathbf{q}_τ and $\bar{\mathbf{q}}_\tau$ do not have a physical interpretation. Figure 7c shows the basins of the sinks of \mathbf{m}_τ and figure 7d does so for the basins of $\bar{\mathbf{m}}_\tau$.

Figure 9b shows the detected 7 sink behavior critical path lines and their corresponding extracted separation surfaces. These critical path lines are sinks in forward integration of \mathbf{v} (marked with blue points), and all the path lines in the area between the critical path line and the surrounding separation surface asymptotically converge to the critical path line when integrated forward. Figure 9c shows the detected 4 source behavior critical path lines and their corresponding extracted separation

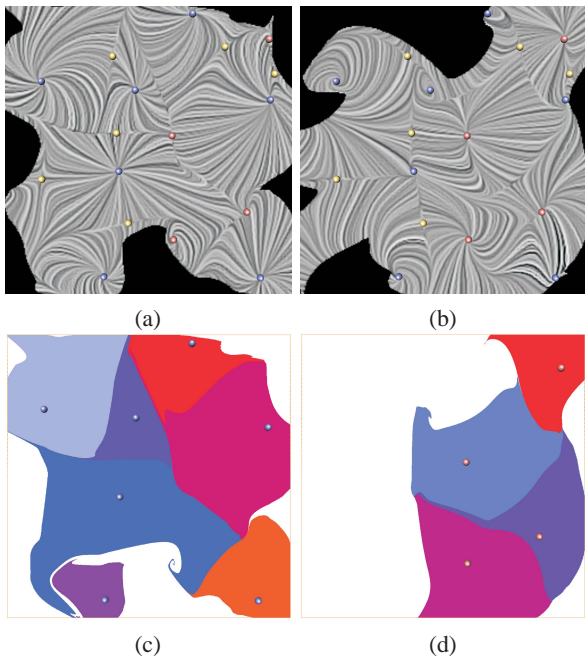


Figure 7: The random data set: (a) \mathbf{q}_τ at $\tau = t_{min}$; (b) $\bar{\mathbf{q}}_\tau$ at $\tau = t_{min}$; (c) Basins of \mathbf{q}_τ at $\tau = t_{min}$; (d) Basins of $\bar{\mathbf{q}}_\tau$ at $\tau = t_{min}$.

surfaces. These critical path lines are sinks in backward integration of \mathbf{v} (marked with red points), and all the path lines in the area between the critical path line and the surrounding separation surface asymptotically converge to the critical path line when integrate backward. The computing time for this data set was 10 minutes for the basin generation, several seconds for seeding curve extraction and 30 minutes for the separation surface integration with 50 integration steps and 8×8 polar stratified super sampling on a Pentium 4 with 3.40 GHz.

Figure 8 and figure 9d-f visualize the path line oriented topology of the electrostatic field around a benzene molecule. This data set was calculated on a 101^3 regular grid using the fractional charges method described in [14]. Originally this is a 3D steady gradient field describing the force of the electrostatic potential upon a positive point charge given in a certain location. If such a point charge is situated very close to the molecule, the closest atom will exert the highest force on it, i.e., attract or repel it. The influence of a single atom decreases the farther the point charge is located from the whole molecule. Instead, all atoms have nearly the same influence. One might say that the molecule as a whole is exerting force on a somewhat far located point charge. Thus, it is possible to distinguish between a near and a far field.

Since the behavior of this field is rather complex [19, 27], we applied our method to find a simplified visual representation by neglecting the w -component of the field and interpreting the z -axis as time. This yields

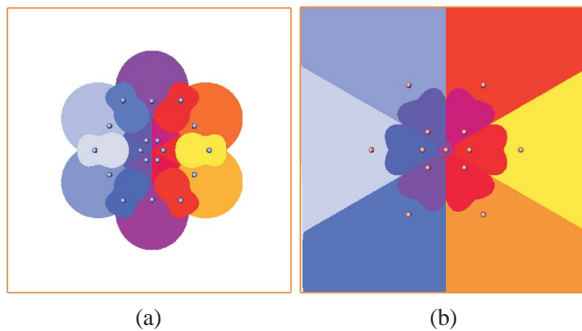


Figure 8: The periodic benzene data set: (a) Basins of \mathbf{q}_τ at $\tau = t_{min}$; (b) Basins of $\bar{\mathbf{q}}_\tau$ at $\tau = t_{min}$.

inside into the forces induced by the *distribution* of the atoms in the main plane of the molecule: as one moves away from the molecule, the influence of a single atom decreases and therefore the influence of the atom distribution decreases as well. The field can now be interpreted as a 2D periodic vector field, since the 2D forces are the same on both sides of the molecule.

Figure 9d elucidates the influence of atom distribution: the trajectories change radically close to the molecule (high influence in near field) while in other areas they are nearly straight (low influence in far field). To get insight into the attracting and repelling behavior, we computed the basins for forward and backward integration (figure 8) as well as their corresponding critical path lines (figures 9e-f).

Figure 9e shows the 18 sink behavior critical path lines and their corresponding extracted separation surfaces for periodic benzene force field. All the point charges in the area between the critical path line and the surrounding separation surface asymptotically converge to the critical path line as time goes. Similarly figure 9f shows the 13 sink behavior critical path lines and their corresponding extracted separation surfaces. All the point charges in the area between the critical path line and the surrounding separation surface asymptotically converge to the critical path line for backward integration. The computing time for benzene data set was 15 minutes for the basin generation, several seconds for seeding curve extraction and 100 minutes for the separation surface integration with 80 integration steps and 8×8 polar stratified super sampling.

7 CONCLUSIONS

In this paper we introduced an approach to extracting the separation surfaces for asymptotic behavior of path lines in periodic time-dependent vector fields. We apply an image analysis method to extract the seeding curves and integrate these seeding curves with step advancing super sampling adjustment to generate the final separation surfaces. The main limitation of our separation surface extraction approach is that the basin shape must be contiguous enough. If they are quite irregular and dis-

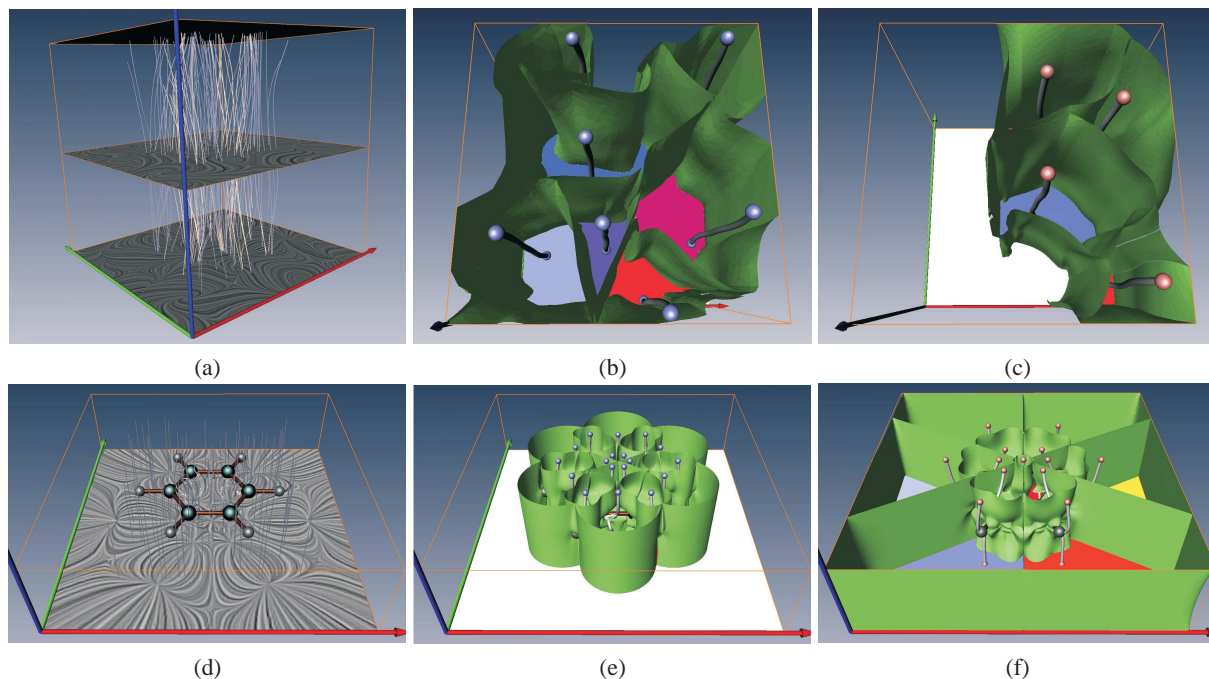


Figure 9: (a) The visualization of a random periodic vector field and the corresponding path lines; (b) The forward converge separation surfaces and the corresponding sink critical path lines for the random data set; (c) The backward converge separation surfaces and the corresponding source critical path lines for the random data set; (d) The visualization of the periodic benzene force field, the benzene molecule and the corresponding path lines; (e) The forward converge separation surfaces and the corresponding sink critical path lines for the benzene data set; (f) The backward converge separation surfaces and the corresponding source critical path lines for the benzene data set.

continuous, the seeding curve extraction will fail. However the basins of many applications are regular enough to extract the separation surfaces.

ACKNOWLEDGMENT

All visualizations in this paper have been created using AMIRA – a system for advanced 3D visualization and volume modeling [15] (see <http://amira.zib.de/>). The project has partially been supported by Max Planck Center of Visual Computing and Communication (MPC-VCC). Parts of this work have been done in the scope of the basic research on visualization at the VRVis Research Center in Vienna, Austria, which is funded by an Austrian research program called Kplus.

REFERENCES

- [1] W. de Leeuw and R. van Liere. Collapsing flow topology using area metrics. In *Proc. IEEE Visualization '99*, pages 149–354, 1999.
- [2] W. de Leeuw and R. van Liere. Visualization of global flow structures using multiple levels of topology. In *Data Visualization 1999. Proc. Vis-Sym 99*, pages 45–52, 1999.
- [3] C. Garth, X. Tricoche, and G. Scheuermann. Tracking of vector field singularities in unstruc-
- [4] A. Globus, C. Levit, and T. Lasinski. A tool for visualizing the topology of three-dimensional vector fields. In *Proc. IEEE Visualization '91*, pages 33–40, 1991.
- [5] R. C. Gonzalez and R. E. Woods. *Digital Image Processing*. Addison-Wesley, 3rd edition, 1992.
- [6] J. Helman and L. Hesselink. Representation and display of vector field topology in fluid flow data sets. *IEEE Computer*, 22(8):27–36, August 1989.
- [7] R. C. Jain, R. Kasturi, and B. G. Schunck. *Machine Vision*. McGraw-Hill, 1995.
- [8] S.K. Lodha, J.C. Renteria, and K.M. Roskin. Topology preserving compression of 2D vector fields. In *Proc. IEEE Visualization 2000*, pages 343–350, 2000.
- [9] H. Löffelmann, H. Doleisch, and E. Gröller. Visualizing dynamical systems near critical points. In *Spring Conference on Computer Graphics and its Applications*, pages 175–184, Budmerice, Slovakia, 1998.
- [10] H. Löffelmann, T. Kučera, and E. Gröller. Visualizing Poincaré maps together with the underlying flow. In *Proc. VisMath '97*, pages 315–328, 1998.

- [11] K. Mahrous, J. Bennett, G. Scheuermann, B. Hamann, and K. Joy. Topological segmentation in three-dimensional vector fields. *IEEE Transactions on Visualization and Computer Graphics*, 10(2):198–205, 2004.
- [12] G. Scheuermann, H. Krüger, M. Menzel, and A. Rockwood. Visualizing non-linear vector field topology. *IEEE Transactions on Visualization and Computer Graphics*, 4(2):109–116, 1998.
- [13] K. Shi, H. Theisel, T. Weinkauff, H. Hauser, H.-C. Hege, and H.-P. Seidel. Path line oriented topology for periodic 2d time-dependent vector fields. In *Data Visualization 2006. Proc. EuroVis '06*, pages 139–146, 2006.
- [14] D. Stalling and T. Steinke. Visualization of vector fields in quantum chemistry. Technical report, ZIB Preprint SC-96-01, 1996. <ftp://ftp.zib.de/pub/zib-publications/reports/SC-96-01.ps>.
- [15] D. Stalling, M. Westerhoff, and H.-C. Hege. Amira: A highly interactive system for visual data analysis. *The Visualization Handbook*, pages 749–767, 2005.
- [16] H. Theisel. Designing 2D vector fields of arbitrary topology. *Computer Graphics Forum (Eurographics 2002)*, 21(3):595–604, 2002.
- [17] H. Theisel, Ch. Rössl, and H.-P. Seidel. Compression of 2D vector fields under guaranteed topology preservation. *Computer Graphics Forum (Eurographics 2003)*, 22(3):333–342, 2003.
- [18] H. Theisel and H.-P. Seidel. Feature flow fields. In *Data Visualization 2003. Proc. VisSym 03*, pages 141–148, 2003.
- [19] H. Theisel, T. Weinkauff, H.-C. Hege, and H.-P. Seidel. Saddle connectors - an approach to visualizing the topological skeleton of complex 3D vector fields. In *Proc. IEEE Visualization 2003*, pages 225–232, 2003.
- [20] H. Theisel, T. Weinkauff, H.-C. Hege, and H.-P. Seidel. Topological methods for 2D time-dependent vector fields based on stream lines and path lines. *IEEE Transactions on Visualization and Computer Graphics*, 11(4):383–394, 2005.
- [21] X. Tricoche, G. Scheuermann, and H. Hagen. A topology simplification method for 2D vector fields. In *Proc. IEEE Visualization 2000*, pages 359–366, 2000.
- [22] X. Tricoche, G. Scheuermann, and H. Hagen. Continuous topology simplification of planar vector fields. In *Proc. Visualization 01*, pages 159 – 166, 2001.
- [23] X. Tricoche, T. Wischgoll, G. Scheuermann, and H. Hagen. Topology tracking for the visualization of time-dependent two-dimensional flows. *Computers & Graphics*, 26:249–257, 2002.
- [24] B. Wallisch. Internet-based visualization of basin boundaries for three-dimensional dynamical systems, 2000.
- [25] T. Weinkauff, H. Theisel, H.-C. Hege, and H.-P. Seidel. Boundary switch connectors for topological visualization of complex 3D vector fields. In *Data Visualization 2004. Proc. VisSym 04*, pages 183–192, 2004.
- [26] T. Weinkauff, H. Theisel, H.-C. Hege, and H.-P. Seidel. Topological construction and visualization of higher order 3D vector fields. *Computer Graphics Forum (Eurographics 2004)*, 23(3):469–478, 2004.
- [27] T. Weinkauff, H. Theisel, K. Shi, H.-C. Hege, and H.-P. Seidel. Extracting higher order critical points and topological simplification of 3D vector fields. In *IEEE Visualization*, page 71. IEEE Computer Society, 2005.
- [28] T. Weinkauff, H. Theisel, K. Shi, H.-C. Hege, and H.-P. Seidel. Topological simplification of 3d vector fields by extracting higher order critical points. In *Proc. IEEE Visualization 2005*, pages 559–566, 2005.
- [29] R. Westermann, C. Johnson, and T. Ertl. Topology-preserving smoothing of vector fields. *IEEE Transactions on Visualization and Computer Graphics*, 7(3):222–229, 2001.
- [30] T. Wischgoll and G. Scheuermann. Detection and visualization of closed streamlines in planar flows. *IEEE Transactions on Visualization and Computer Graphics*, 7(2):165–172, 2001.
- [31] T. Wischgoll, G. Scheuermann, and H. Hagen. Tracking closed stream lines in time-dependent planar flows. In *Proc. Vision, Modeling and Visualization 2001*, pages 447–454, 2001.